



Effect of the bivalent dopant ionic radius, electronegativity and concentration on the physical properties of the sol–gel-derived ZnO thin films

Rabab Bekkari¹ · Larbi Laârab¹ · Boujemaâ Jaber²

Received: 14 May 2020 / Accepted: 22 July 2020 / Published online: 31 July 2020
© Springer Science+Business Media, LLC, part of Springer Nature 2020

Abstract

This study deals with the influence of the concentration and ionic radius of the bivalent dopant on the structural, morphological and optical properties of the sol–gel-derived ZnO thin films. For that, different concentrations of dopants with different radii (Ni^{2+} , Cu^{2+} , Fe^{2+}) have been chosen to synthesize many ZnO thin films. The X-ray diffraction confirms that all the obtained films exhibit a pure hexagonal wurtzite structure. Meanwhile, it appears that both the preferential film orientation and the crystal quality are strongly affected when varying the ionic radius or the concentration of dopant. We note also that the lattice parameters decrease when the electronegativity of the dopant increases. This behavior has been explained at the light of a simple schematic model, based on the electrostatic forces involved in chemical bonding. The Scherer formula reveals that the average size of the crystallites is ranged between 20 and 35 nm. On the other hand, as confirmed by the SEM analysis, all the deposited films present a compact, uniform and nanocrystalline morphology. Nonetheless, the optical analysis indicates that the Ni- and Fe-doped films are highly transparent (greater than 90%) in the visible region, while the Cu-doped ones exhibit the lowest transmission (about 76%). Additionally, a blue shift of the bandgap is noticed when doping with Ni or Fe, whereas the doping with Cu induces a red shift.

1 Introduction

Zinc oxide (ZnO) is an attractive n-type semiconductor and technologically important due to its unique properties as piezoelectric [1], wide bandgap (3.37 eV) [2], transparent in the visible [3] and can be made to conduct with suitable dopants [4]. Its piezoelectric properties are exploited in thin-film applications for surface acoustic wave devices [5] and transducers [6]. Furthermore, its tunable bandgap and high transparency have made ZnO an ideal material useful for short-wavelength and transparent optoelectronic devices including UV lasers [7, 8], LED [9–11], transparent electrodes [12] as well as window layers [13, 14] in the solar cells.

However, in order to enhance the physical behavior of ZnO as a versatile material for the above applications, doping is one of the effective approaches that makes this material an excellent subject for theoretical and experimental studies. In fact, doping ZnO with selective elements offers an effective method to improve and control its electrical, structural, magnetic and optical properties [15]. In general, the efficiency of one dopant depends strongly on its electronegativity, concentration and ionic radius, which need to be optimized to afford different industrial criteria.

Recently, a wide variety of 3d transition metals such as Mo [16], Ni [17, 18], Co [19], Ti [20], Cu [21–23] and Fe [24] were tested as dopants in ZnO to improve its optical and electrical behaviors for many applications. Although various deposition methods have been developed to produce doped ZnO, the effect of dopant concentration on ZnO lattice is still not clear and very controverting. Furthermore, it is well known that ZnO thin films with hexagonal wurtzite structure crystallize preferentially along the *c*-axis orientation which allows the development of transducers operating only in the longitudinal mode. Consequently, many researchers have studied the influence of diverse parameters on the final properties of ZnO thin films, particularly the doping effect. For

✉ Rabab Bekkari
bekkarirabab@gmail.com

¹ LCS, Faculty of Science, Mohammed V University in Rabat, Rabat, Morocco

² UATRS Division, Materials Science Platform, CNRST, Rabat, Morocco

instance, Cu-doped ZnO thin films prepared by the sol–gel method: Gómez-Pozos et al. [22], using two copper precursors, have noticed that the films were nanocrystalline in nature with a hexagonal phase having (002) preferential orientation. On the contrary, Jongnavakit et al. [23] by varying Cu concentrations (0.1, 0.3, 0.5, 0.7 and 1%) revealed that all samples were polycrystalline with no preferential orientation whatever the Cu concentration may be. On the other hand, Kim et al. [18] elaborated Ni-doped ZnO thin films (0.2, 0.4, 0.6 and 0.8%) by sol–gel process. They found that NZO thin films with a dopant ratio (0.2 and 0.4%) have a preferred orientation in the (002) direction. However, when the Ni doping ratio exceeds 0.6%, films possessed a non-textured polycrystalline structure. However, as it has been reported, the ZnO piezoelectric properties are directly affected by the crystallite orientation control in the film [25, 26]. Hereafter, when seeking to develop ZnO-based transducers, it is more suitable to drive ZnO growing along orientations other than the habitual *c*-axis one. In fact, exclusively in this case, both the longitudinal and transverse modes could be excited. Up to now and to our knowledge, the control of the ZnO films orientation by doping has not yet been studied.

In this framework, the main novelty of this work is to investigate the growth orientation control of sol–gel-derived ZnO thin films, by varying the ionic radius, electronegativity and concentration of the bivalent dopant. The main objective of this study is to make the excitation of all ZnO vibration modes possible and efficient, which will positively impact the technology and the quality of piezoelectric transducers. Through this work, we project also to understand the effect of the bivalent dopant on the ZnO host lattice parameters. For that, an original schematic model, based on the difference of electronegativity, has been proposed and discussed. In this respect, the influence of different bivalent dopants (Ni^{2+} , Cu^{2+} , Fe^{2+}), with different ionic radii, electronegativities and concentrations, on the structural, morphological and optical properties of the sol–gel-derived ZnO thin films, has been investigated and discussed.

2 Experimental

The sol–gel spin coating method has been used to prepare undoped and doped ZnO films with different bivalent elements (Ni, Cu and Fe). In the synthesis process, we have used zinc acetate dihydrate [$\text{Zn}(\text{CH}_3\text{CO}_2)_2 \cdot 2\text{H}_2\text{O}$], isopropanol [$\text{C}_3\text{H}_8\text{O}$], monoethanolamine [MEA, $\text{C}_2\text{H}_7\text{NO}$] and nickel acetate [$\text{Ni}(\text{CH}_3\text{COO})_2 \cdot 4\text{H}_2\text{O}$], copper (II) acetate monohydrate [$\text{Cu}(\text{CH}_3\text{COO})_2 \cdot \text{H}_2\text{O}$] as well as iron II Chloride [$\text{FeCl}_2 \cdot 6\text{H}_2\text{O}$] as a precursor of zinc, solvent, stabilizer and source of dopants, respectively. Firstly, the zinc acetate dihydrate was dissolved in a mixture of isopropanol and MEA, and then the solution was heated at 60 °C for one

hour before adding dopant at chosen concentration. The zinc acetate concentration in solution was kept at 0.5 M and the molar ratio of MEA/Zinc was maintained at 1. A clear homogeneous solution was obtained after one hour of reaction. The ZnO films were then deposited on the glass substrates by spin coating at 3000 rpm for 30 s under normal conditions of temperature and pressure. The other experimental details are described in our previous work [27].

The crystalline structure was analyzed by Panalytical Expert Pro X-Ray Diffractometer working in Bragg–Brentano geometry with Cu $K\alpha$ radiation. Surface morphology was examined using a JEOL Scanning Electron Microscopy (JSM-IT100) coupled to a microanalysis EDS system. UV–Vis transmittance spectra were recorded using a Perkin Elmer lambda 900 spectrophotometer at room temperature in the wavelength range of 300–800 nm.

3 Results and discussion

3.1 Effect of the ionic radius and electronegativity

To investigate the effect of the ionic radius and electronegativity on the physical properties, many ZnO films, doped with ions of different radii (Ni^{2+} (0.69 Å), Cu^{2+} (0.72 Å) and Fe^{2+} (0.74 Å)) and electronegativity (Ni^{2+} (1.91), Cu^{2+} (1.90) and Fe^{2+} (1.83)) at a fixed concentration of 5%, were synthesized.

3.2 Structural properties

XRD analyses of the undoped and doped ZnO thin films, presented in Fig. 1a, show that all the films are of hexagonal wurtzite structure, without any additional secondary dopant-related phase (JCPDS card No.: 01-089-7102). In order to show the dopant impact on the ZnO crystal lattice, Fig. 1b illustrates the XRD data zoom in the 30° to 38° angular range. As can be seen, when the ionic radius decreases ($\text{Fe}^{2+} \rightarrow \text{Cu}^{2+} \rightarrow \text{Ni}^{2+}$), a peak shift towards higher angles is clearly observed, indicating a decrease in the lattice parameters. This kind of shift is likely due to the effective substitution of Zn by dopant atoms in the ZnO matrix [28–30].

To quantify the orientation tendency of the obtained ZnO films, the peak ratios were used. The variation of the peak ratios as a function of the dopant ionic radius is presented in Fig. 1c. It is clear that, when compared to the bulk, the intensity of (002) peak increases in detriment of (101) when the dopant ionic radius decreases ($\text{Fe}^{2+} \rightarrow \text{Cu}^{2+} \rightarrow \text{Ni}^{2+}$). These results confirm that the ZnO growth orientation depends clearly on the bivalent dopant ionic radius.

The crystallite size (*D*) of the films, given in Table 1, was calculated from XRD data using the Debye–Scherrer formula:

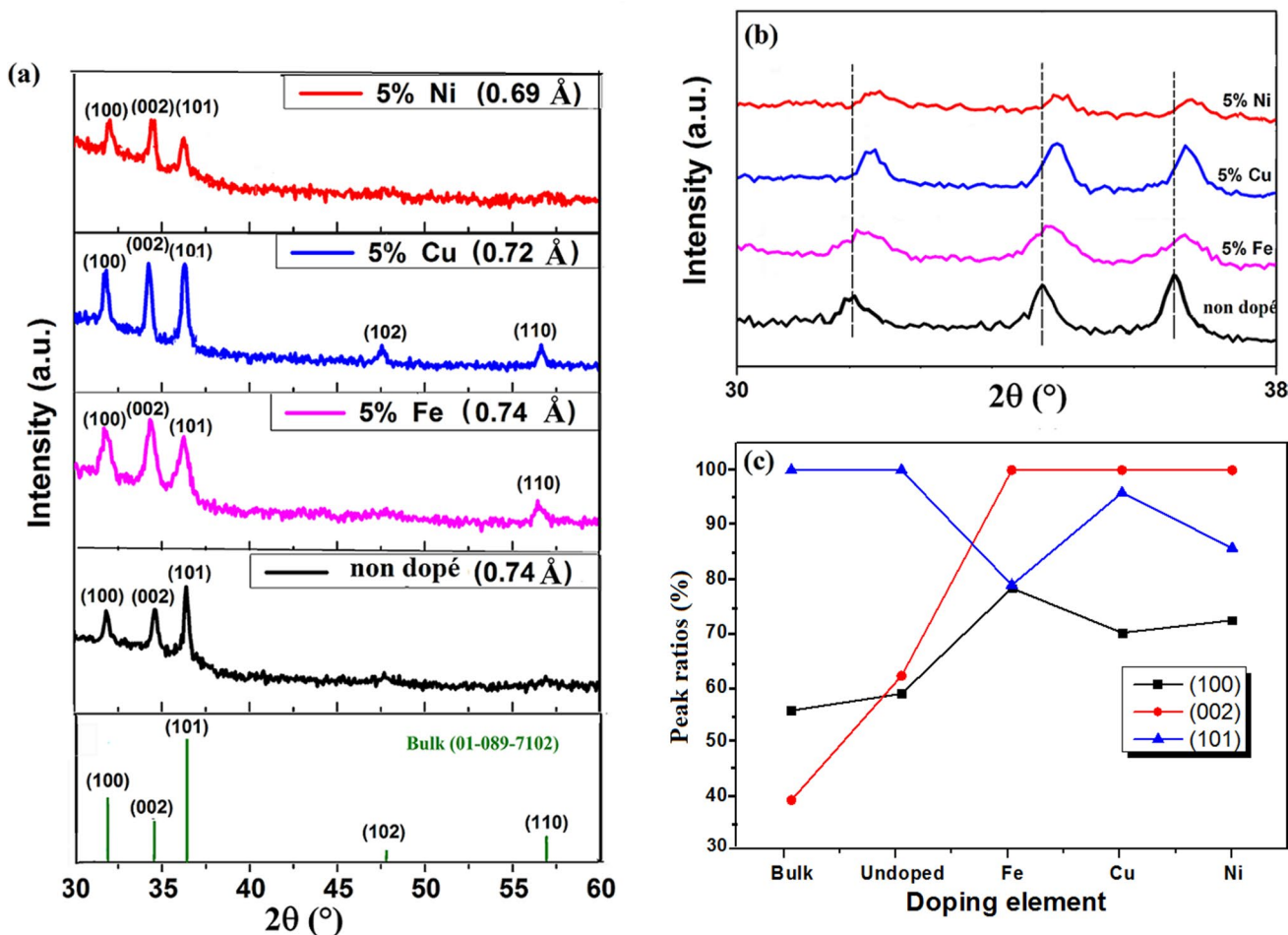


Fig. 1 X-ray diffraction diagrams (a), the position of the ZnO hexagonal structure diffraction peaks (b) and the relative intensity ratio (c) of undoped and doped ZnO thin films with bivalent elements of different ionic radii (Ni²⁺, Cu²⁺ and Fe²⁺)

Table 1 Structural parameters of the undoped ZnO thin film as well as Ni-, Cu- and Fe-doped ZnO thin films

Doping elements	Ionic radius (Å)	χ	crystallite size (nm)	Lattice parameters (Å)		L (Å)	σ (GPa)
				a	c		
Undoped	0.74	1.65	35	3.2553 ± 0.0006	5.2128 ± 0.0008	1.9810	-0.3045
Fe	0.74	1.83	25	3.2470 ± 0.0006	5.2031 ± 0.0009	1.9762	0.1260
Cu	0.72	1.90	21	3.2360 ± 0.0006	5.1830 ± 0.0008	1.9692	1.0254
Ni	0.69	1.91	20	3.2330 ± 0.0006	5.1817 ± 0.0009	1.9669	1.1320

$$D = \frac{0.9\lambda}{\beta \cos \theta}, \tag{1}$$

where λ is the wavelength of the used X-ray radiation (1.5406 Å); β is the full width at half maximum (FWHM) and θ is the Bragg diffraction angle. According to these values, the crystallites size decreases slightly when the dopant changes in the following sequence: Fe → Cu → Ni. Since no significant difference in the ionic radius of the dopants, compared to that of Zn²⁺, we think that the observed variation of

crystallites size is rather linked to the electronegativity variation of the doping element. To better clarify this tendency, we present in Fig. 2, the variation of the obtained Scherrer’s crystallite size as a function of the dopant electronegativity. As can be observed, when the electronegativity of the dopant increases the crystallite size decreases linearly. This important result shows that increasing the dopant electronegativity affects negatively the crystallites growth kinetics and then blocks the grain boundary mobility.

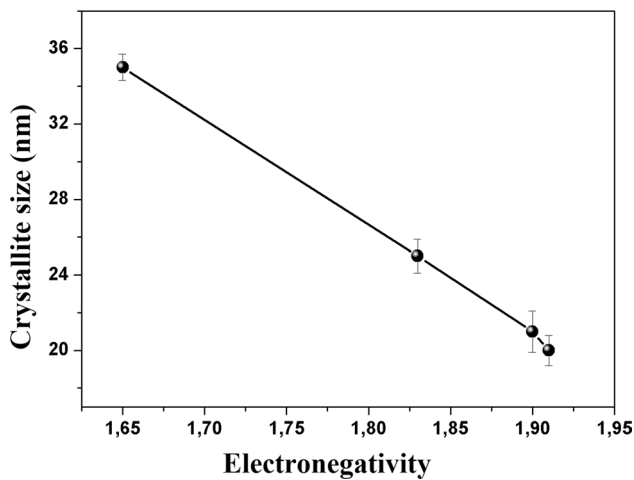


Fig. 2 Crystallite size variation of undoped and doped ZnO thin films with Ni, Cu and Fe as a function of electronegativity

For wurtzite phase, a and c lattice parameters can be calculated by using Bragg's law:

$$a = \frac{\lambda}{\sqrt{3} \sin \theta_{(100)}} \quad (2)$$

$$c = \frac{\lambda}{\sin \theta_{(002)}} \quad (3)$$

In the same way, the Zn–O bond length (L) is given by the equation:

$$L = \sqrt{\frac{a^2}{3} + \left(\frac{1}{2} - u\right)^2 c^2} \quad (4)$$

$$\text{with } u = \frac{a^2}{3c^2} + \frac{1}{4} \quad (5)$$

As reported in Table 1, an eminent decrease of the lattice parameters occurs when changing the dopants as follows: Fe → Cu → Ni. As the Fe²⁺, Cu²⁺ and Ni²⁺ ionic radii are comparable to that of Zn²⁺, we believe that the observed decrease of a and c parameters, when changing the Fe → Cu → Ni dopant, is evidently associated to the increase of their electronegativity. As illustrated in Fig. 3, a remarkable decrease in the a and c parameters is noticed when the dopant electronegativity increases from 1.65 to 1.91. To provide more explanation about this behavior, Table 1 presents also the values of the Zn–O bond length (L) calculated for each studied dopant. Since electronegativity is defined as the ability of an atom to attract electrons, the higher the electronegativity, the stronger the attraction of the electrons. Based on this rule, as schematically modeled in Fig. 4, when the dopant electronegativity increases, the attraction on the electron cloud of oxygen

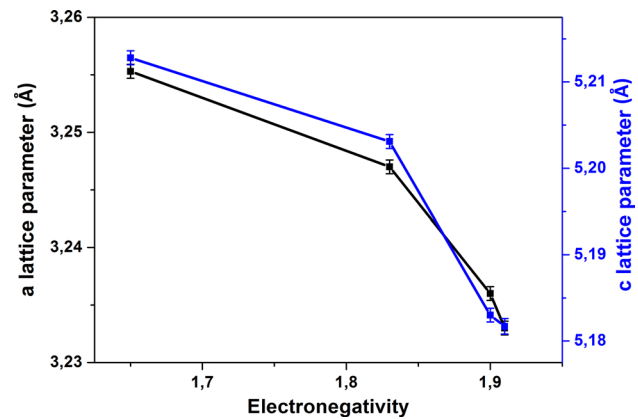


Fig. 3 Variation of lattice parameters a and c of undoped and doped ZnO thin films with Ni, Cu and Fe as a function of electronegativity

becomes higher, and therefore the bond length (or the lattice parameter) is reduced as illustrated in Table 1.

On the other hand, the stresses in ZnO-doped thin films can be determined using the following equation:

$$\sigma = (2C_{13}^2 - C_{33}(C_{11} + C_{12})) \times \left(\frac{\varepsilon}{2C_{33}} \right) \quad (6)$$

The elastic constants of single-crystalline ZnO $C_{11}=208.8$, $C_{12}=119.7$, $C_{13}=104.2$ and $C_{33}=213.8$ GPa have been used [31]. ε is the strain along the c -axis. The results presented in Table 1 show that, as the electronegativity of the dopant changes from 1.65 to 1.91, the value of the stress in the doped ZnO thin films varies from -0.3045 to 1.1320 GPa. The positive values of the computed stresses for the Ni-, Cu- and Fe-doped samples indicate that they are tensile stresses and present lattice constants little than that of the undoped sample.

3.3 Morphological properties

In order to examine the morphology of pure and doped ZnO thin films with 5% of Cu or Fe, SEM micrographs are shown in Fig. 5a–c. A compact, uniform and nanocrystalline morphology is observed on all the deposited films, indicating a good crystalline quality.

A typical EDS spectrum of the Fe-doped ZnO thin film is presented in Fig. 6. The atomic percentage of Zn, Fe and O elements, given in Table 2, confirms an amount of Fe equal to (4.40%) which is very close to the nominal composition (5%).

3.4 Optical properties

Figure 7 displays the optical transmittance spectra of the undoped and doped ZnO thin films with Ni, Cu and Fe. It is clear that the Ni-doped film is highly transparent (about 96%) in the visible region (400–800 nm) and

Fig. 4 Schematic model explaining the variation of the dopant-oxygen bond length as a function of the dopant electronegativity

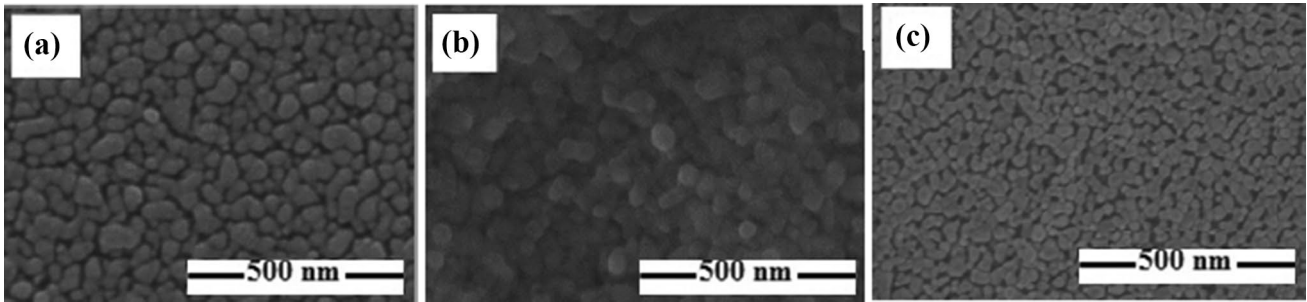
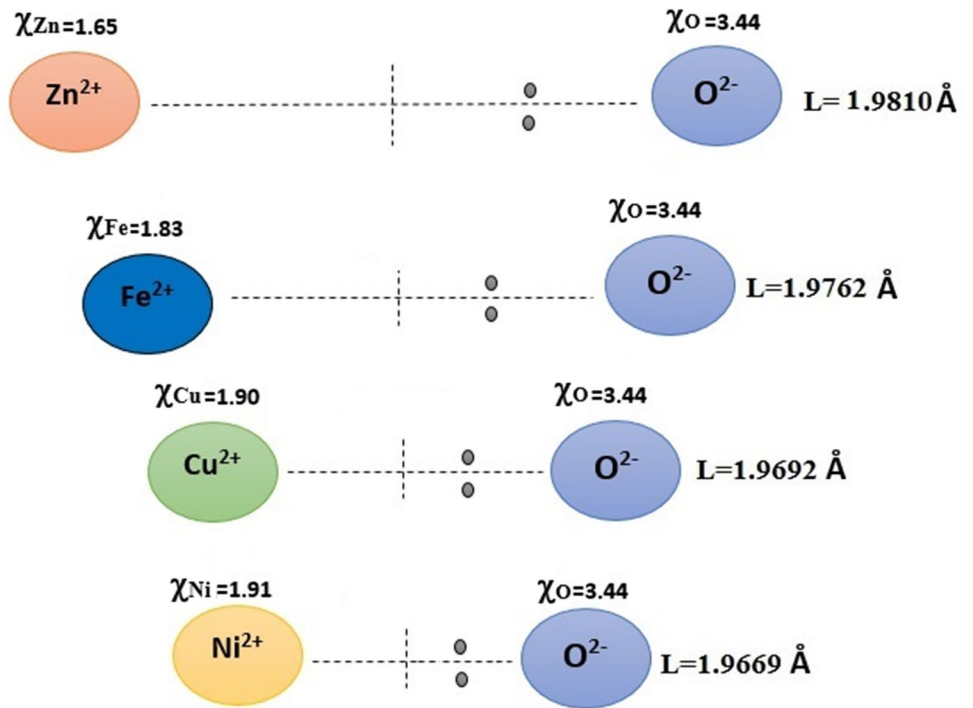


Fig. 5 SEM images of undoped (a) and doped ZnO thin films at 5% with Fe (b) and Cu (c)

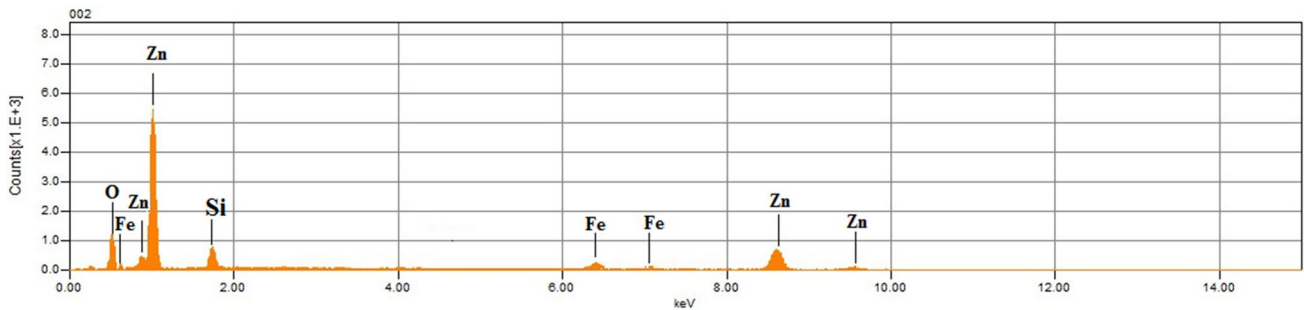


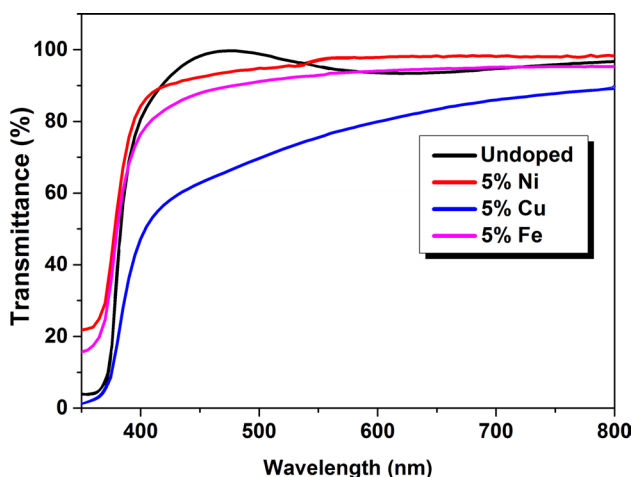
Fig. 6 EDS spectrum of a typical 5% Fe-doped ZnO thin film

presents a sharp falling of the absorption edge in the UV region (350–400 nm), while that doped with Cu exhibits a minimum value of transmission (about 76%) with a net

fundamental absorption edge. Meanwhile, the observed decreases of the doped film transmittance in the visible and in the UV ranges could be attributed to the increase of the

Table 2 Atomic percentages of Zn, Fe and O elements in the 5% Fe-doped film

Sample	At.%		
	O	Zn	Fe
ZnO:Fe	46.79	48.81	4.40

**Fig. 7** UV-Vis transmittance spectra of undoped and doped ZnO thin films

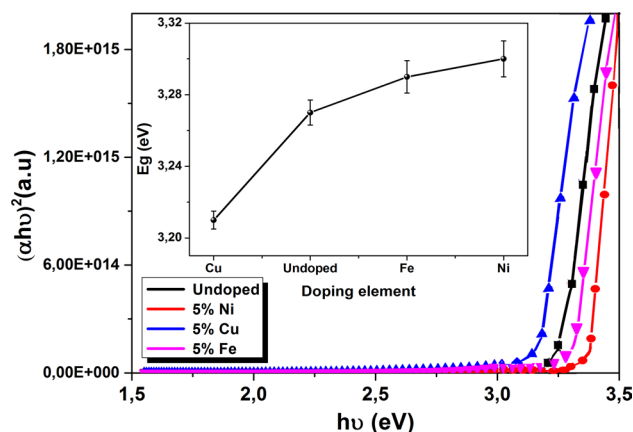
film thickness [32, 33]. It is worth noting that the Ni and Fe spectra present also a blue shift of the absorption edge, indicating a slight widening of the optical window of these films. Contrarily, this trend ceases to be valid when doping with copper for which a red shift is observed.

The optical bandgap energy of the films assuming a direct transition is evaluated by the extrapolation of the linear portion of $(\alpha h\nu)^2$ versus $h\nu$ plots using Tauc formula:

$$\alpha h\nu = A(h\nu - E_g)^{1/2}, \quad (7)$$

where α is the absorption coefficient, $h\nu$ is the photon energy, A is a constant, and E_g is the optical bandgap energy. The Tauc plot $(\alpha h\nu)^2$ versus $(h\nu)$ of undoped and doped ZnO thin films is presented in Fig. 8. From the plots, it is observed that the gap energy changes with the dopants. It increases when doping with Ni or Fe and decreases when doping with Cu. The observed increase of the E_g in the case of Ni- or Fe-doped films may be ascribed to the small crystallites size. However, despite of the small crystallites size, the observed decrease of the E_g when doping with Cu could be attributed to (i) the strong coupling between the orbital d of Cu and the orbital p of O, and/or (ii) the Cu 3d orbital creates impurity bands overhead the ZnO valence band [34–36].

In conclusion of this paragraph, the X-ray diffraction patterns show that all undoped and doped deposited films are polycrystalline with a wurtzite hexagonal structure. In addition, a slight reduction of the dopant ionic radius results in a

**Fig. 8** Plot of $(\alpha h\nu)^2$ versus $h\nu$ of undoped and doped ZnO thin films with different elements

net increase of the (002) peak in detriment of the (101) one. It is then possible to control the growth orientation, through doping, which is beneficial when seeking to design ultrasonic transducers operating in transverse and longitudinal modes. The Ni- and Fe-doped films are highly transparent (greater than 90%) and exhibit a blue shift, while that doped with Cu has a low transmission (about 76%) with a red shift.

3.5 Effect of Cu and Ni concentration

According to the last study, doping with Ni or Fe presents the same behavior, which is different from that related to the Cu doping. To better understand this difference, we study in this section the effect of Ni and Cu doping concentration on the structural and optical properties of ZnO thin films. For that, Ni- and Cu-doped ZnO samples have been elaborated with different concentrations (0, 1, 5 and 10%).

3.6 Structural properties

Figures 9a and 10a show the XRD diagrams of the undoped and doped ZnO thin films with Cu and Ni at different concentrations. The polycrystalline nature of the hexagonal wurtzite structure of ZnO is confirmed. The diffraction peaks can be identified as (100), (002) and (101) planes according to JCPDS # 01-089-7102. Except the characteristic peaks of ZnO, no additional peak corresponding to Copper or Nickel has been detected. Additionally, Figs. 9b and 10b show that the diffraction peaks of ZnO samples doped with Cu or Ni are shifted to higher angles if the doping rate is increased beyond 1% for Cu and 5% for the Ni. This shift can be explained by the decrease of the lattice parameters occurred subsequently to the effective substitution of Zn by the doping atoms in the ZnO matrix.

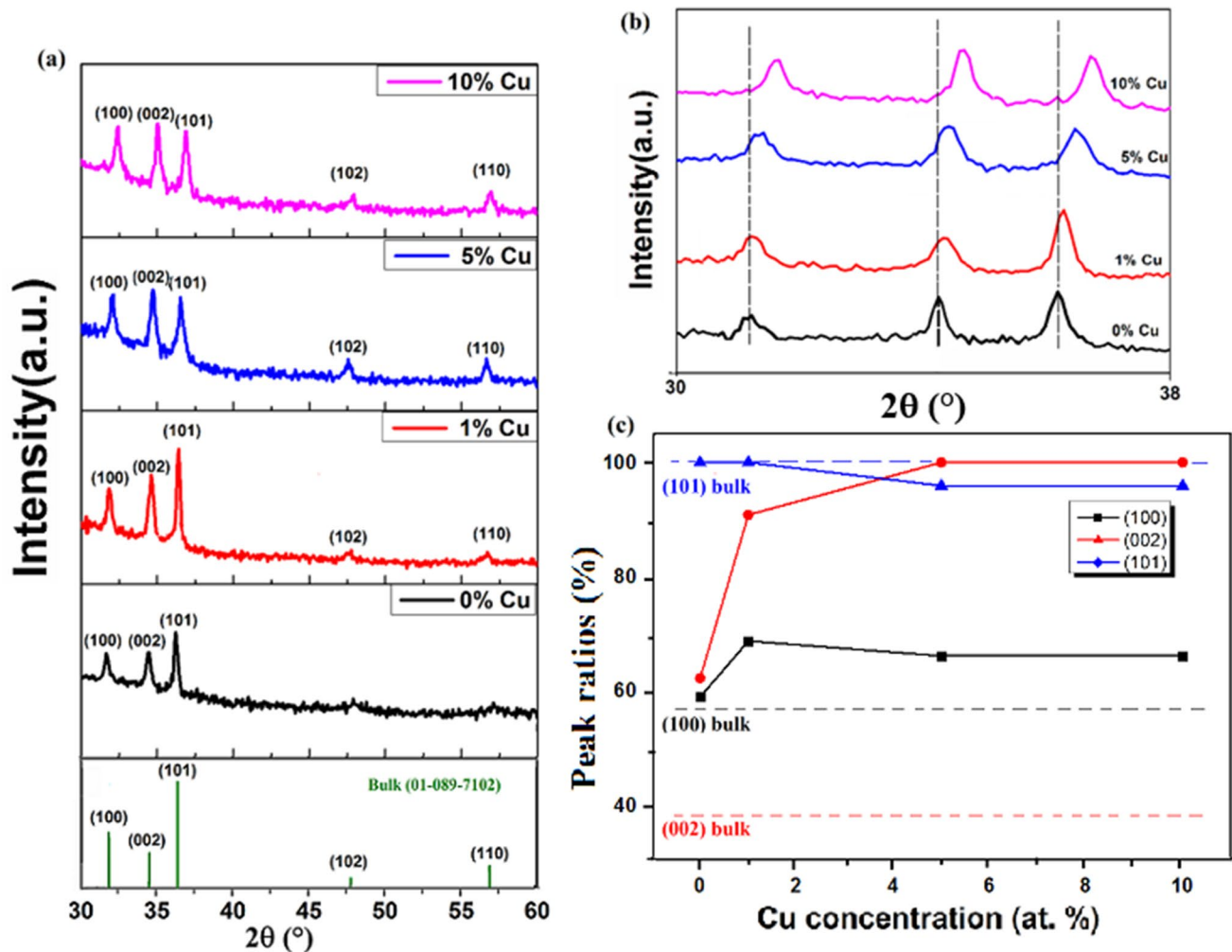


Fig. 9 X-ray diffraction patterns of CZO (a), the position of diffraction peaks of CZO (b), the relative intensity ratio of CZO (c) thin films with different concentrations of Cu doping

Otherwise, the variations of the peak ratios as a function of the concentration of Cu and Ni are presented in Figs. 9c and 10c. When the Cu concentration varies from 0 to 1%, Fig. 9c shows a significant increase in the intensity of the (100), (002) and (101) peaks. However, for higher concentrations, a slight decreasing trend followed by a remarkable stability of the intensity is observed and this for all the plans. According to the literature [37, 38], the observed improvement of the crystalline quality at low doping concentrations can be explained through the creation of new nucleation centers involving doping atoms. However, the decrease followed by a stability of the peak intensity observed in higher doping concentrations is probably due to the saturation of these new nucleation centers. In fact, the excess copper undergoes segregation in grain boundaries and thus retards and then blocks the grain growth process [37, 39].

Concerning the nickel, we present in Fig. 10c the variations of the peak ratios as a function of the concentration.

For the low concentrations of Ni, this figure shows that the intensity of (100), (101) and (002) peaks decreases. However, for the high concentrations, the intensity of (002) increases, while those of (101) and (100) peaks decrease. We can deduce that a high concentration of Ni favors the (002) preferential orientation. This behavior can be understood since the ionic radius of Ni^{2+} (0.69 Å) is smaller than that of Zn^{2+} (0.74 Å), at low concentration, Ni occupies only interstitial sites, and then the peaks intensities decrease [40]. Meanwhile, at high concentrations these interstitial sites become saturated, the Ni then occupies the substitutional sites which results in the increases of the (002) intensity.

On the other side, based on the XRD results of Figs. 9 and 10 the structural characteristics have been estimated for different Cu and Ni concentrations and summarized in Table 3.

These calculations show that the crystallites size and lattice parameters exhibit different behaviors depending on the Ni and Cu concentration. On one hand, when the dopant

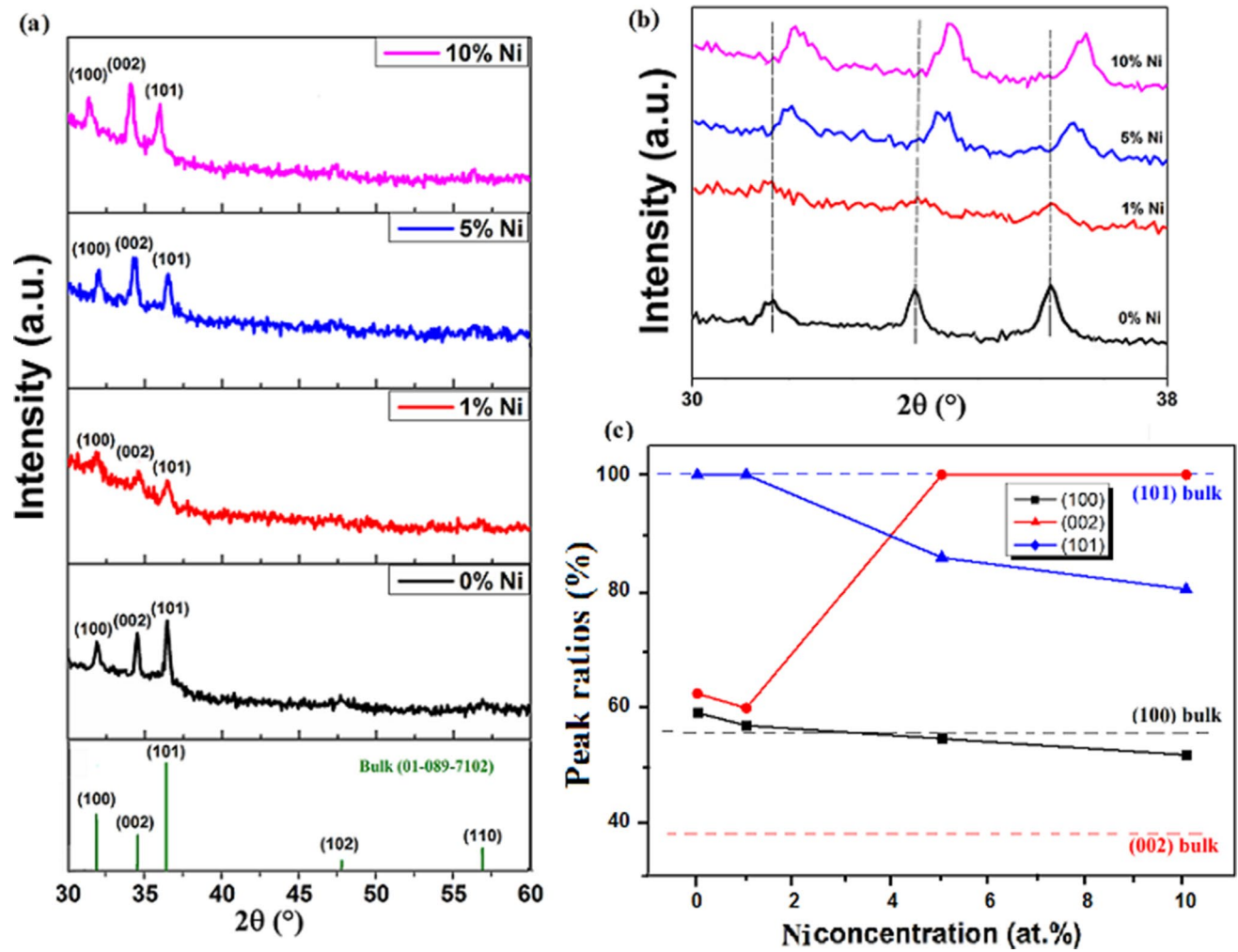


Fig. 10 X-ray diffraction patterns of NZO (a), the position of diffraction peaks of NZO (b), the relative intensity ratio of NZO (c) thin films with different concentrations of Ni doping

concentration increases, a slight decrease in the crystallite size is observed in both Cu- and Ni-doped samples. This retard of growth observed at high concentration may be explained by the fact that the excess doping atoms could exert drag forces on boundary motion and grain growth [37, 41], which result in small crystallite sizes.

On the other hand, no remarkable change in the lattice parameters has been observed for Ni at low concentration (1%). However, these parameters exhibit a net decrease at relatively high concentrations (from 5 to 10%) (Table 3). We think that, because of its small ionic radius, Ni occupies only interstitial sites at low concentration; its incorporation

Table 3 Various structural parameters of ZnO thin films doped with Cu or Ni

Cu and Ni content (%)	Crystallite size (nm)		Lattice parameters (Å)				σ (GPa)	
	CZO	NZO	CZO		NZO		CZO	NZO
			<i>a</i>	<i>c</i>	<i>a</i>	<i>c</i>		
0	35	35	3.2553 ± 0.0006	5.2128 ± 0.0008	3.2553 ± 0.0006	5.2128 ± 0.0008	-0.3045	-0.3045
1	28	26	3.2483 ± 0.0006	5.2018 ± 0.0008	3.2544 ± 0.0006	5.2123 ± 0.0009	0.1873	-0.2857
5	21	20	3.2399 ± 0.0006	5.1889 ± 0.0008	3.2330 ± 0.0006	5.1807 ± 0.0009	0.7650	1.1320
10	23	20	3.2225 ± 0.0006	5.1772 ± 0.0008	3.2200 ± 0.0005	5.1717 ± 0.0008	1.2878	1.5353

therefore induces no expansion in the ZnO lattice. Contrariwise, the reduction in the lattice parameters observed at high concentration (greater than 5%) indicates clearly that the interstitial sites become saturated and that the excess of Ni passes into substitution. In the case of CZO films, it is worth noting that the both a and c parameters decrease even though at low Cu concentration (1%). This reduction can be attributed to the Cu ionic radius which is slightly greater than that of Ni. In fact, contrary to Ni, the Cu atoms, which cannot be hosted in interstitial sites, go directly into substitution even for low concentration. The small difference in the ionic radius between Zn and Cu is at the origin of the observed lattice parameters reduction. Note also that the increase in the concentration of the two dopants induces the increase of the stress, as shown by the results presented in Table 3.

3.7 Optical properties

In order to understand the doping concentration effect on the optical properties, we have reported in Fig. 11a and b the optical transmission spectra of the ZnO films elaborated at different Cu and Ni doping rates. The measured average transmittances and thicknesses of the doped films are reported in Table 4. A significant reduction of the transmittance (from 92 to 73%), in the 400–800 nm range, is observed as the Cu doping rate increases up to 10% (Fig. 11a). This reduction of transmittance is due to the observed increase of the film thickness (Table 4). Meanwhile, a slight improvement of the transmittance (from 92 to 96%) associated to a net decrease of the film thickness (Fig. 11b and Table 4) is noticed, in the case of NZO films, as the Ni concentration is varied similarly up to 10%. This last behavior makes this material quite suitable as a window for solar cells.

Table 4 Average optical transmittance of doped ZnO films in the visible range and films thickness as a function of doping concentration

Doping concentration (%)	CZO		NZO	
	Film thickness (nm)	Average transmittance (%)	Film thickness (nm)	Average transmittance (%)
0	363	92	363	92
1	370	91	322	93
5	419	76	298	94
10	425	74	275	96

At this point, we can notice that the transmittance manifests dissimilar behaviors, and that depends on the nature and concentration of the dopant.

The observed reduction of transmittance in the case of CZO films is attributed to (i) the highest viscosity of the prepared sol, when compared to that of the NZO films. In fact, the increase in Cu doping induces an augmentation in the solution viscosity that raises the deposition rate and consequently increases the thickness of the film, which decreases the transmittance of the film [35]; and/or (ii) to the crystallographic orientation of the films. In fact, it has been reported that a maximum optical transmittance is characteristic of a preferentially oriented material along the c -axis, because of the reduced amount of optical scattering in the grain boundaries. However, a poly-oriented structure would have reduced transmittance due to the excessive dispersion of light in the joints [42].

Figure 12a and b displays the variations of $(\alpha h\nu)^2$ with photon energy $h\nu$ for CZO and NZO films. This figure presents also the variation of bandgap energy with doping concentration. Again, two antagonist tendencies are observed. On one side, increasing the Cu concentration results in a

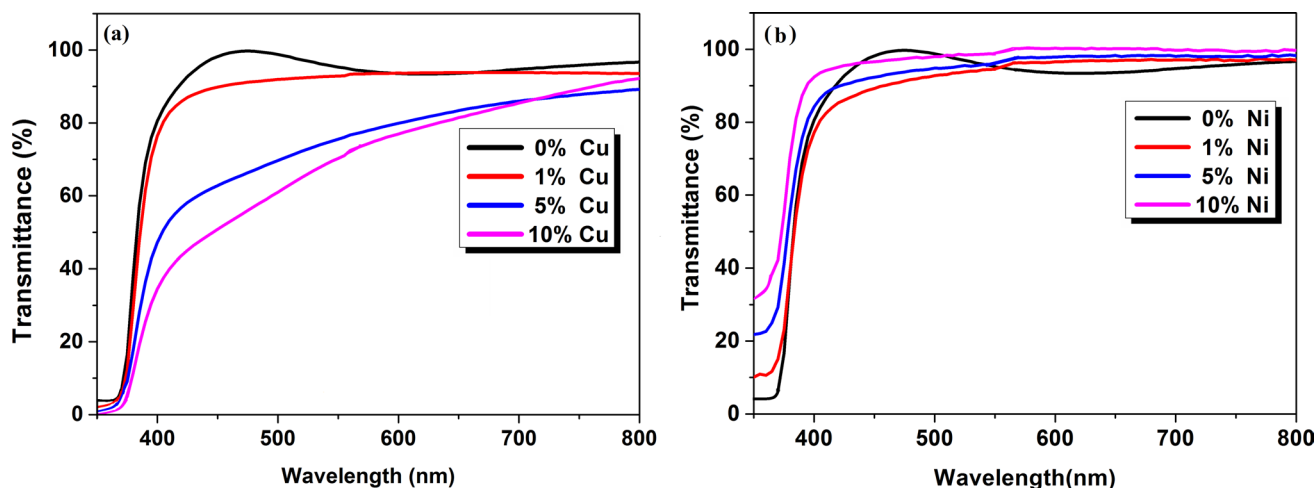


Fig. 11 Transmittance spectra of undoped and doped ZnO thin films at different contents of Cu (a) and Ni (b)

remarkable reduction of E_g . This reduction may be attributed to (i) the strong coupling between the orbital d of the Cu atom and the orbital p of the O atom, which results in an enlargement of the valence band, (ii) the Cu 3d orbital makes impurity bands overhead the ZnO valence band [34–36]. On the other, we emphasize that E_g does not undergo any variation in the 0–1% doping range in the case of NZO films. This result is in agreement with the structural study in which we show no variation of the lattice parameters in this doping range because the Ni occupies only the interstitial sites. Beyond 1%, these interstitial sites became saturated and the Ni passes into substitution, which causes a reduction in the lattice parameters associated with an enlargement of the bandgap. In the same way, the observed increase of E_g with increasing the Ni concentration could also be explained through the Burstein–Moss effect [43]. Indeed, with a high p doping concentration, the semiconductor becomes degenerated and the Fermi level enters the valence band. Since the position of the latter depends on the concentration of the dopants, as the Ni content increases, the highest electronic states in the valence band become vacant and, therefore, shift the absorption edge towards higher photon energy [44].

At the end of this second comparative study, we conclude that the undoped and doped ZnO thin films with Cu and Ni have a polycrystalline nature with a hexagonal wurtzite structure without any secondary phase. Low-concentration Cu doping improves the crystalline quality and decreases the lattice parameters. However, low-concentration Ni doping affects negatively the crystalline quality and has no evident effect on the lattice parameters. However, high Cu concentration results in a remarkable decrease in both the crystalline quality and the lattice parameters; contrariwise, a high concentration of Ni improves the crystalline quality by favoring the preferential orientation (002) and reduces the lattice parameters. Optical analysis shows that the doping

with Cu results in a reduction of the transmittance in the visible region with a red shift of the optical gap from 3.27 to 3.17 eV, though the doping with Ni improves the transmittance and engenders a blue shift of the gap from 3.27 to 3.33 eV.

4 Conclusion

In conclusion, the effect of different bivalent dopants on the structural and optical properties of ZnO thin films has been studied and discussed. We opted in this study for Ni^{2+} , Cu^{2+} and Fe^{2+} , having ionic radii slightly different from that of Zn^{2+} , considering that they have different electronegativities which are clearly higher than that of Zn^{2+} . XRD diagrams show that all undoped and doped deposited films are polycrystalline with a hexagonal wurtzite structure. In addition, as the ionic radius of the dopant slightly increases and/or the electronegativity decreases, the (101) peak intensity drops while that of the (002) peak increases. Accordingly to this observation, we can state that it is possible to control the crystallite growth orientation only by varying the electronegativity and/or the ionic radius of the bivalent dopant. This result is of great interest when seeking to design future acoustic transducers, operating in both transverse and longitudinal modes. In a comparative study between Cu^{2+} and Ni^{2+} bivalent dopants, based on XRD, low-concentration Cu doping improves the crystalline quality and decreases the lattice parameters, whereas low-concentration Ni doping affects negatively the crystalline quality and has no evident effect on the lattice parameters. However, high Cu concentration results in a remarkable decrease in both the crystalline quality and the lattice parameters; contrariwise, a high concentration of Ni improves the crystalline quality by favoring the preferential orientation (002) and reduces the

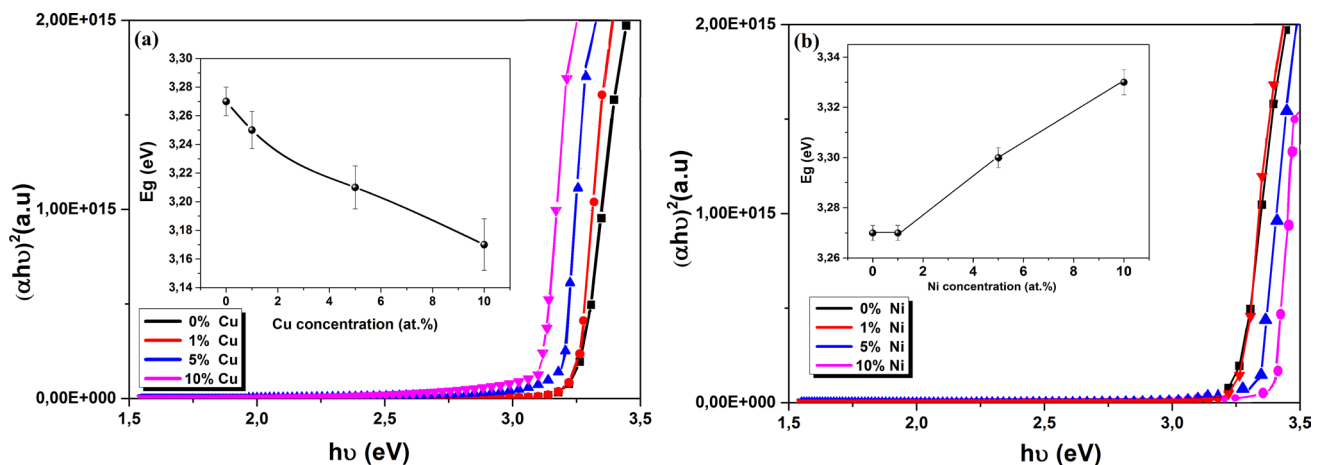


Fig. 12 $(\alpha h\nu)^2$ versus $h\nu$ plots of CZO (a) and NZO (b) thin films at various Cu and Ni contents

lattice parameters. Moreover, the SEM observations indicate a compact, uniform and nanocrystalline morphology of all the deposited films. However, optical analysis reveals that Ni- and Fe-doped films are highly transparent (greater than 90%) with a bandgap blue shift, whereas those doped with Cu^{2+} show a reduced transmission (about 76%) with a bandgap red shift.

Acknowledgements The authors wish to thank the National Center of Scientific and Technical Research (CNRST) and the staff of the UATRS Division, for use of their equipment and technical assistance.

References

- R. Bekkari, L. Laânb, D. Boyer, R. Mahiou, B. Jaber, *Mater. Sci. Semicond. Process.* **71**, 181–187 (2017)
- D. Sivaganesh, S. Saravanakumar, V. Sivakumar, K.S.S. Ali, E. Akapo, E. Alemayehu, R. Rajajeyaganthan, R. Saravanan, *J. Mater. Sci. Mater. Electron.* **30**, 2966 (2019)
- X. Wei, B. Man, C. Xue, C. Chen, M. Liu, *Jpn. J. Appl. Phys.* **45**, 8586 (2006)
- A. Mallick, D. Basak, *Prog. Mater. Sci.* **96**, 86 (2018)
- V.L. Patil, S.A. Vanalakar, P.S. Patil, J.H. Kim, *Sens. Actuators B Chem.* **239**, 1185 (2017)
- R. Haarindraprasad, U. Hashim, S.C.B. Gopinath, M. Kashif, P. Veeradasan, S.R. Balakrishnan, K.L. Foo, P. Poopalan, Y.K. Mishra, *PLoS ONE* **10**, 1 (2015)
- P.S. Shewale, Y.S. Yu, *J. Alloys Compd.* **654**, 79 (2016)
- V. Kumar, O.M. Ntweaborwa, H.C. Swart, *J. Colloid Interface Sci.* **465**, 295 (2016)
- M. Karimipour, M. Sadeghian, M. Molaei, *J. Mater. Sci. Mater. Electron.* **29**, 13782 (2018)
- M. Huang, S. Wang, G. Wan, X. Zhang, Y. Zhang, K. Ou, L. Yi, *J. Mater. Sci. Mater. Electron.* **29**, 7213 (2018)
- M. Xin, *J. Theor. Appl. Phys.* **12**, 177 (2018)
- M. Murugesan, D. Arjunraj, J. Mayandi, V. Venkatachalapathy, J.M. Pearce, *Mater. Lett.* **222**, 50 (2018)
- S. Zhang, N.D. Pham, T. Tesfamichael, J. Bell, H. Wang, *Sustain. Mater. Technol.* **18**, e00078 (2018)
- Z.N. Kayani, H. Bashir, S. Riaz, S. Naseem, *Mater. Res. Bull.* **115**, 121 (2019)
- S.I. Shanthi, S. Poovaragan, M.V. Arularasu, S. Nithya, R. Sundaram, C.M. Magdalane, K. Kaviyarasu, M. Maaza, *J. Nanosci. Nanotechnol.* **18**, 5441 (2018)
- M. Wu, S. Yu, G. Chen, L. He, L. Yang, W. Zhang, *Appl. Surf. Sci.* **324**, 791 (2015)
- T. Wakano, N. Fujimura, Y. Morinaga, N. Abe, A. Ashida, T. Ito, *Phys. E Low-Dimens. Syst. Nanostruct.* **10**, 260 (2001)
- K.T. Kim, G.H. Kim, J.C. Woo, C.I. Kim, *Surf. Coatings Technol.* **202**, 5650 (2008)
- M.G. Nair, M. Nirmala, K. Rekha, A. Anukaliani, *Mater. Lett.* **65**, 1797 (2011)
- H. Chen, J. Ding, S. Ma, *Superlattices Microstruct.* **49**, 176 (2011)
- S. Singhal, J. Kaur, T. Namgyal, R. Sharma, *Phys. B Condens. Matter.* **407**, 1223 (2012)
- H. Gómez-Pozos, E.J.L. Arredondo, A.M. Álvarez, R. Biswal, Y. Kudriavtsev, J.V. Pérez, Y.L. Casallas-Moreno, M.L.O. Amador, *Materials (Basel)* **9**, 87 (2016)
- P. Jongnavakit, P. Amornpitoksuk, S. Suwanboon, N. Ndiege, *Appl. Surf. Sci.* **258**, 8192 (2012)
- U. Alver, T. Kiliç, E. Bacaksiz, S. Nezir, *Mater. Sci. Eng. B Solid-State Mater. Adv. Technol.* **138**, 74 (2007)
- D. Ali, M.Z. Butt, B. Arif, A.A. Al-Ghamdi, F. Yakuphanoglu, *Phys. B Condens. Matter* **506**, 83 (2017)
- O. Dimitrov, D. Nesheva, V. Blaskov, I. Stambolova, S. Vassilev, Z. Levi, V. Tonchev, *Mater. Chem. Phys.* **148**, 712–719 (2014)
- R. Bekkari, B. Jaber, H. Labrim, M. Ouafi, N. Zayyoun, L. Laânb, *Int. J. Photoenergy* **2019**, 1 (2019)
- J.P. Mathew, G. Varghese, J. Mathew, *S.O.P. Trans, Appl. Phys.* **1**, 27 (2014)
- K. Joshi, M. Rawat, S.K. Gautam, R.G. Singh, R.C. Ramola, F. Singh, *J. Alloys Compd.* **680**, 252 (2016)
- T. Srinivasulu, K. Saritha, K.T.R. Reddy, *Mod. Electron. Mater.* **3**, 76–85 (2017)
- B.R. Kumar, T.S. Rao, *Dig. J. Nanomater. Bios.* **6**, 1281 (2011)
- A. Sreedhar, J.H. Kwon, J. Yi, J.S. Kim, J.S. Gwag, *Mater. Sci. Semicond. Process.* **49**, 8 (2016)
- R. Bekkari, L. Laânb, B. Jaber, *J. Chem.* **4**, 2289 (2016)
- A.A. Othman, M.A. Ali, E.M.M. Ibrahim, M.A. Osman, *J. Alloys Compd.* **683**, 399 (2016)
- R. Raji, K.G. Gopchandran, *Mater. Res. Express* **4**, 025002 (2017)
- K. Ahn, T. Deutsch, Y. Yan, C. Jiang, C.L. Perkins, K. Ahn, T. Deutsch, Y. Yan, C. Jiang, C.L. Perkins, J. Turner, M. Al-jassim, *J. Appl. Phys.* **102**, 023517 (2007)
- G. Li, X. Zhu, X. Tang, W. Song, Z. Yang, J. Dai, Y. Sun, X. Pan, S. Dai, *J. Alloys Compd.* **509**, 4816 (2011)
- M. Öztas, M. Bedir, *Thin Solid Films* **516**, 1703 (2008)
- G. Li, X. Zhu, H. Lei, W. Song, Z. Yang, J. Dai, Y. Sun, X. Pan, S. Dai, *J. Alloys Compd.* **505**, 434 (2010)
- F. Boudjouan, A. Chelouche, T. Touam, D. Djouadi, Y. Ouerdane, *Mater. Sci. Semicond. Process.* **41**, 382–389 (2016)
- J.A. Najim, J.M. Rozaiq, *Int. Lett. Chem. Phys. Astron.* **15**, 137 (2013)
- Y.S. Kim, W.P. Tai, S.J. Shu, *Thin Solid Films* **491**, 153 (2005)
- R.K. Rajakarthy, S. Muthukumaran, *Opt. Mater. (Amst.)* **69**, 382–391 (2017)
- R.A. Rakkesh, S. Balakumar, *Process. Appl. Ceram.* **8**, 7–13 (2014)

Publisher's Note Springer Nature remains neutral with regard to jurisdictional claims in published maps and institutional affiliations.